J. Fluid Mech. (2022), *vol*. 933, A55, doi:10.1017/jfm.2021.1109

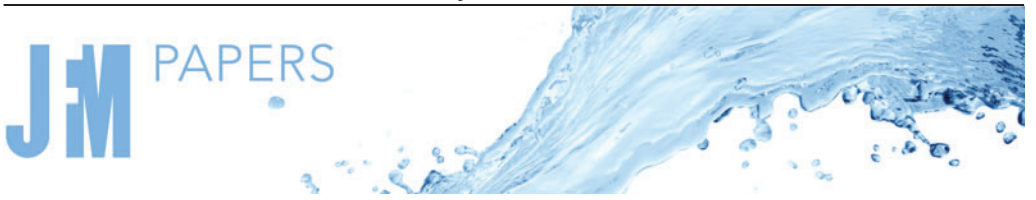

Linear stability of a rotating liquid column revisited

Pulkit Dubey[1,2], Anubhab Roy[3] and Ganesh Subramanian[2,†]

[1]Integrated Applied Mathematics Program, University of New Hampshire, Durham, NH 03824, USA

[2]Engineering Mechanics Unit, JNCASR, Bangalore, Karnataka 560064, India

[3]Department of Applied Mechanics, Indian Institute of Technology Madras, Chennai, Tamil Nadu 600036, India

(Received 28 July 2021; revised 30 October 2021; accepted 7 December 2021)

We revisit the somewhat classical problem of the linear stability of a rigidly rotating liquid column in this article. Although the literature pertaining to this problem dates back to 1959, the relation between inviscid and viscous stability criteria has not yet been clarified. While the viscous criterion for stability, given by $We < n^2 + k^2 - 1$, is both necessary and sufficient, this relation has only been shown to be sufficient in the inviscid case. Here, $We = \rho\Omega^2 a^3/\gamma$ is the Weber number and measures the relative magnitudes of the centrifugal and surface tension forces, with Ω being the angular velocity of the rigidly rotating column, a the column radius, ρ the density of the fluid and γ the surface tension coefficient; k and n denote the axial and azimuthal wavenumbers of the imposed perturbation. We show that the subtle difference between the inviscid and viscous criteria arises from the surprisingly complicated picture of inviscid stability in the We–k plane. For all $n > 1$, the viscously unstable region, corresponding to $We > n^2 + k^2 - 1$, contains an infinite hierarchy of inviscidly stable islands ending in cusps, with a dominant leading island. Only the dominant island, now infinite in extent along the We axis, persists for $n = 1$. This picture may be understood, based on the underlying eigenspectrum, as arising from the cascade of coalescences between a retrograde mode, that is the continuation of the cograde surface-tension-driven mode across the zero Doppler frequency point, and successive retrograde Coriolis modes constituting an infinite hierarchy.

Key words: capillary waves, vortex instability

† Email address for correspondence: sganesh@jncasr.ac.in

1. Introduction

This article discusses the linear stability of a rigidly rotating liquid column. The limit of zero rotation corresponds to the classical Rayleigh–Plateau problem analysed first, in the inviscid limit, by Plateau (1873) and later by Rayleigh (1878). The subsequent literature on the rigidly rotating liquid column (Hocking & Michael 1959; Hocking 1960; Gillis & Kaufman 1962; Pedley 1967) primarily focused on the necessary and/or sufficient condition for instability, although later Weidman, Goto & Fridberg (1997) examined the dominant unstable modes for the inviscid rotating column based on growth-rate calculations. More recently, Kubitschek & Weidman (2007*a*) obtained the dominant modes for the viscous rotating column, and organized their results based on the wavenumber of the dominant perturbation, in a parameter plane consisting of the Weber number (a dimensionless measure of rotation defined below) and the column Reynolds number. The boundaries demarcating the crossover of the dominant mode in this plane converged smoothly to the inviscid predictions of Weidman *et al.* (1997) for $Re \to \infty$. The later experiments of Kubitschek & Weidman (2007*b*) were consistent with the modal crossover boundaries obtained in Kubitschek & Weidman (2007*a*). While all of the above results show the expected destabilizing effect of rotation, in terms of a larger range of wavenumbers turning unstable with an increase in the column angular velocity, on account of centrifugal forces, there remains a difference between the viscous and inviscid criteria for instability obtained in the early literature (Hocking & Michael 1959; Hocking 1960; Gillis & Kaufman 1962; Pedley 1967). Although the expression for the stability threshold (see (2.5) below) remains the same in both cases, it has been shown to be necessary and sufficient in the presence of viscosity (Gillis & Kaufman 1962), but only serves as a sufficient condition in the inviscid limit (Pedley 1967; Weidman 1994; Henderson & Barenghi 2002). In this article, we re-examine the instability of a rigidly rotating liquid column, with an emphasis on the entire inviscid spectrum, including the neutral modes. The analysis sheds new light on this problem, showing that inviscid unstable modes arise from an infinite hierarchy of coalescences between pairs of dispersion curves just above the viscous threshold. The resulting intricate picture helps explain the aforementioned difference between the nature of the inviscid and viscous threshold criteria.

Perturbations to a liquid column may be characterized in terms of their azimuthal (n) and axial (k) wavenumbers and, accordingly, may be classified as axisymmetric ($n = 0$, $k \neq 0$), planar ($n \neq 0, k = 0$) and helical (spiral) or three-dimensional perturbations ($n \neq 0, k \neq 0$). Starting in § 2, we study the dispersion curves, and the associated stability thresholds, for a rigidly rotating column of liquid subject to each of the aforementioned classes of perturbations. The nature of the dispersion curves is a function of the Weber number, $We = \rho\Omega^2 a^3/\gamma$, a dimensionless parameter that compares the relative importance of centrifugal and surface tension forces; here, ρ is the density, Ω the column angular velocity, a the column radius and γ the coefficient of surface tension. For helical perturbations, we analyse the dispersion curves in the We–k plane for different fixed n values. Note that, following early work by Hocking & Michael (1959) and Hocking (1960), We^{-1} has often been referred to as the Hocking parameter (L); for instance, the aforementioned efforts of Weidman *et al.* (1997) and Kubitschek & Weidman (2007*a*) presented their results for the dominant inviscid modes as a function of L, and the dominant viscous modes in the L–Re plane, respectively. In what follows, we stick to We. In the next paragraph, we begin by recapitulating the well known results for the classical case of a stationary liquid column ($We = 0$).

The classical Rayleigh–Plateau instability is one of a stationary liquid column to sufficiently long wavelength axisymmetric perturbations, and explains the spontaneous breakup of a (slow) jet into nearly uniformly sized droplets (see Chandrasekhar (1981); for sufficiently slow speeds, the shear at the air–water interface is unimportant, and the jet may be made equivalent to a stationary column via a Galilean transformation). Plateau (1873) concluded, via a quasistatic analysis, that perturbations with an axial wavelength greater than the circumference of the column ($ka < 1$ or, if the wavenumber is scaled with the column radius, $k < 1$) act to destabilize the column by decreasing the total interfacial area. Rayleigh (1878) then accounted for both inertia and surface tension, obtaining the following dispersion relation for small amplitude Fourier mode perturbations, proportional to $\exp(\mathrm{i}(kx + n\theta - \sigma t))$, in the inviscid limit:

$$\sigma^2 = k\frac{\mathrm{I}_n'(k)}{\mathrm{I}_n(k)}(k^2 + n^2 - 1), \tag{1.1}$$

where $\sigma = \sigma_r + \mathrm{i}\sigma_i$ has been scaled with $\sqrt{\gamma/\rho a^3}$ (σ_r being the frequency and σ_i being the growth rate), and the axial wavenumber (k) is now scaled with $1/a$; $\mathrm{I}_n(k)$ is the modified Bessel function of the first kind with the prime denoting differentiation. From (1.1), only axisymmetric perturbations are found to be unstable ($\sigma_i > 0$) for $k < 1$, with the maximum growth rate corresponding to $k = 0.697$. The growing and decaying modes transform to a pair of neutral modes across $k = 1$, the latter corresponding to capillary waves propagating in opposite directions along the axis of the column. For $k \to \infty$, one obtains $\sigma = \sqrt{\gamma k^3/\rho}$ regardless of n, which is the dispersion relation for capillary waves propagating on an infinite plane interface.

Hocking & Michael (1959) and Hocking (1960) first investigated the effects of rotation on a liquid column subject to planar and axisymmetric perturbations, obtaining the necessary and sufficient criteria for stability. For the axisymmetric case, the authors obtained the criterion $We < k^2 - 1$, regardless of viscosity. For the planar case, the authors found the inviscid criterion to be $We < n(n+1)$, while that for any finite viscosity to be $We < n^2 - 1$ (see also Gillis 1961). Gillis & Kaufman (1962) later studied three-dimensional perturbations of a viscous rotating column and concluded that the latter criterion generalizes to $We < k^2 + n^2 - 1$. Pedley (1967) showed that although the aforementioned viscous criterion remains relevant in the inviscid limit, it only serves as a sufficient condition for stability. Thus, for inviscid columns, a necessary and sufficient condition is not yet known, and clarifying the above difference between the viscous and inviscid criteria is the subject of this effort. As stated above, our focus on the entire eigenspectrum allows us to understand in detail the regions in parameter space corresponding to the inviscid unstable modes while also pointing to the necessary and sufficient criterion for inviscid stability.

While the main findings of the present effort pertain to helical perturbations, we nevertheless consider all three classes of perturbations mentioned above, in sequence, and a complete picture of linear stability emerges as a consequence. Thus, § 2 below starts off with a brief description of the linear stability formulation, which is then followed by subsections pertaining to axisymmetric (§ 2.1) and planar (§ 2.2) perturbations. We detail our new findings for three-dimensional perturbations in § 2.3. In the conclusions section (§ 3), we show that our findings with regard to the non-trivial nature of the inviscid spectrum carry over to the case where the interfacial cohesion underlying surface tension is replaced by a volumetric cohesion mechanism, that of self-gravitation, instead.

This makes our findings relevant to the astrophysical scenario, and we end with a few pertinent comments in that regard.

2. The rotating liquid column

The rigidly rotating columnar base state corresponds to $u_r = 0$, $u_\theta = \Omega r$, $u_z = 0$ and $p = p_0 + (\rho\Omega^2 r^2/2)$ for $r < a$, where p_o is an arbitrary baseline pressure on account of incompressibility. The governing linearized equations for small-amplitude perturbations may be derived in the usual way from the Euler equations, with kinematic (radial velocity) and dynamic (pressure) boundary conditions at the column free-surface. The equations governing inviscid evolution have already been written down and solved in earlier efforts (Hocking & Michael 1959; Hocking 1960; Weidman *et al.* 1997), and in what follows, we directly examine the resulting dispersion relations. Note that the density of the exterior fluid is assumed to be small relative to that of the liquid column, and its influence on column oscillations is neglected.

2.1. *Axisymmetric perturbations*

The dispersion relation for axisymmetric perturbations was obtained by Hocking (1960), and is given by

$$We\,\sigma^2\sqrt{\frac{4}{\sigma^2}-1}\frac{\mathrm{J}_0(\alpha)}{\mathrm{J}_1(\alpha)} - k(k^2-1) + We\,k = 0, \tag{2.1}$$

where $\alpha = k\sqrt{4/\sigma^2 - 1}$. Here, as before, k is scaled with $1/a$ but σ is scaled with Ω as opposed to $\sqrt{\gamma k^3/\rho}$ used in (1.1). Using (2.1), Hocking obtained the necessary and sufficient criterion for stability to be

$$We < k^2 - 1 \tag{2.2}$$

indicating that centrifugal forces destabilize the system, increasing the interval of unstable wavenumbers from (0, 1) in the non-rotating case to $(0, \sqrt{1 + We})$ in the rotating case.

Figure 1(*c*) shows the dispersion curves for the axisymmetrically perturbed column obtained from (2.1). The spectrum is seen to borrow its traits from two constituent cases – the Rayleigh–Plateau configuration involving only surface tension (figure 1*a*) and the Rankine vortex involving only rotation (figure 1*b*). Much like the Rankine vortex, the rotating liquid column supports an infinite sequence of primarily Coriolis-force-driven modes (henceforth referred to as the Coriolis modes), with the inner dispersion curves corresponding to perturbations with an increasingly fine-scaled radial structure; note that the Rankine vortex has recently been shown to also possess a continuous spectrum on account of the irrotational shear in the column exterior (Roy & Subramanian 2014; Roy *et al.* 2021). The Coriolis modes in both these problems have frequencies $\sigma_r \in (-2, 2)$. Additionally, the rotating liquid column has two modes that owe their origin to surface tension akin to the Rayleigh–Plateau configuration (henceforth referred to as the capillary modes). Figure 1(*c*) shows the family of Coriolis modes along with the two capillary modes, and their variation with k, for $We = 20$. Note that the pair of capillary modes follow the characteristic $k^{3/2}$ scaling for large k, while the Coriolis mode frequencies approach $\sigma_r = \pm 2$ in this limit. The effect of We on the dispersion curves is illustrated in figure 2. For $k \ll \sqrt{We + 1}$, Coriolis forces dominate the spectrum, and it is only for $k > \sqrt{We + 1}$ that the effects of surface tension become apparent, with the pair of capillary mode dispersion curves transitioning to the aforementioned $k^{3/2}$ scaling. For $We \gg k^2 - 1$, (2.1)

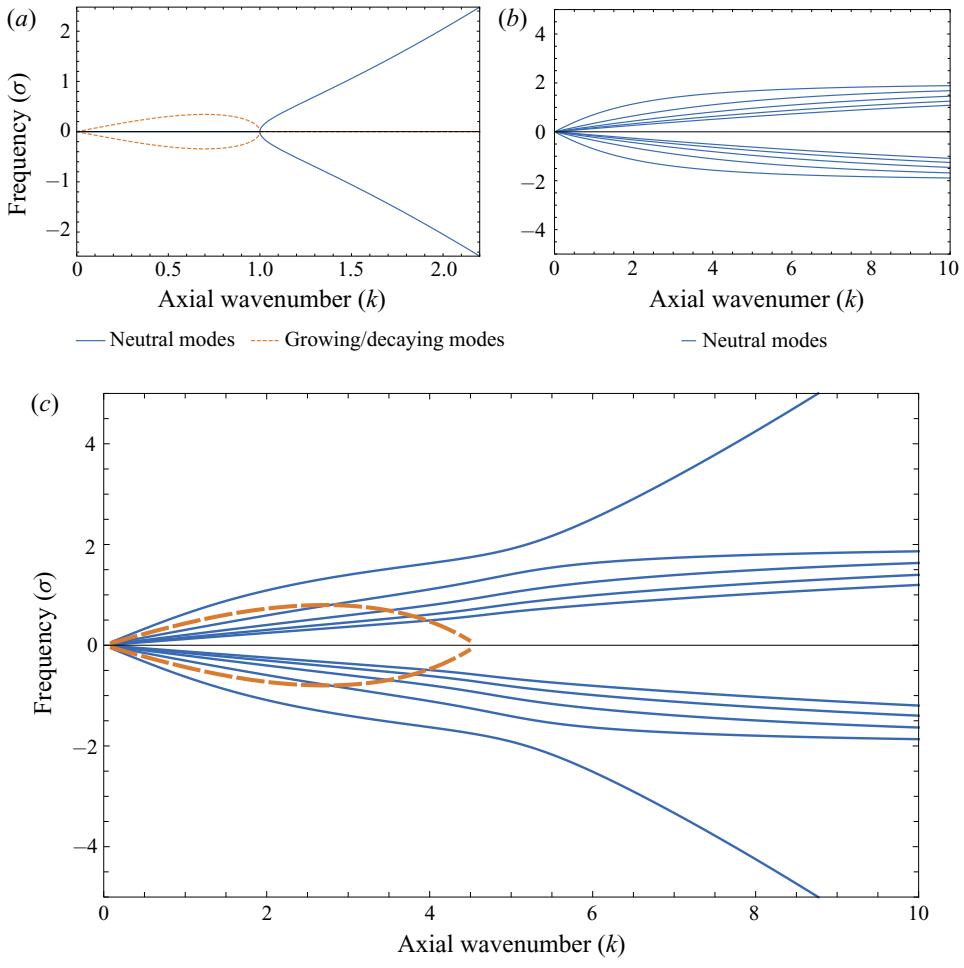

Figure 1. The dispersion curves for the Rayleigh–Plateau problem (*a*), the Rankine vortex (*b*) and the rotating liquid column with $We = 20$ (*c*). Blue curves denote neutral modes while the dotted orange curves denote growing/decaying modes. Only the first 10 of the infinite number of neutral modes are shown for the Rankine vortex and the rotating column.

reduces to $\sigma^2\sqrt{4/\sigma^2 - 1}(\mathrm{J}_0(\alpha)/\mathrm{J}_1(\alpha)) + k = 0$, a *We*-independent dispersion relation; the transition k has receded to infinity and the entire spectrum is governed by Coriolis forces.

Before discussing the spectrum further, we note that while the dispersion relation in (2.1) is in a form suitable for making connections with prior results, and for examining limiting scenarios, it is necessary to use an alternate form, obtained from multiplying all terms in (2.1) by $\mathrm{J}_1(\alpha)$, when plotting the dispersion curves using a software such as Mathematica. Not doing so leads to Mathematica erroneously interpreting the singularities of (2.1), corresponding to the zeros of J_1, as additional zeros, in turn leading to spurious dispersion curves. Similar remarks apply to the dispersion relation for non-axisymmetric modes analysed below (see (2.6)).

The description above clearly shows that there is a qualitative change in the nature of the eigenspectrum with the onset of rotation, as evident from comparing figures 1(*a*) and 1(*c*), and points to the stationary column ($We \to 0$) being a singular limiting case. The interfacial dynamics for the stationary column is entirely determined by the pair

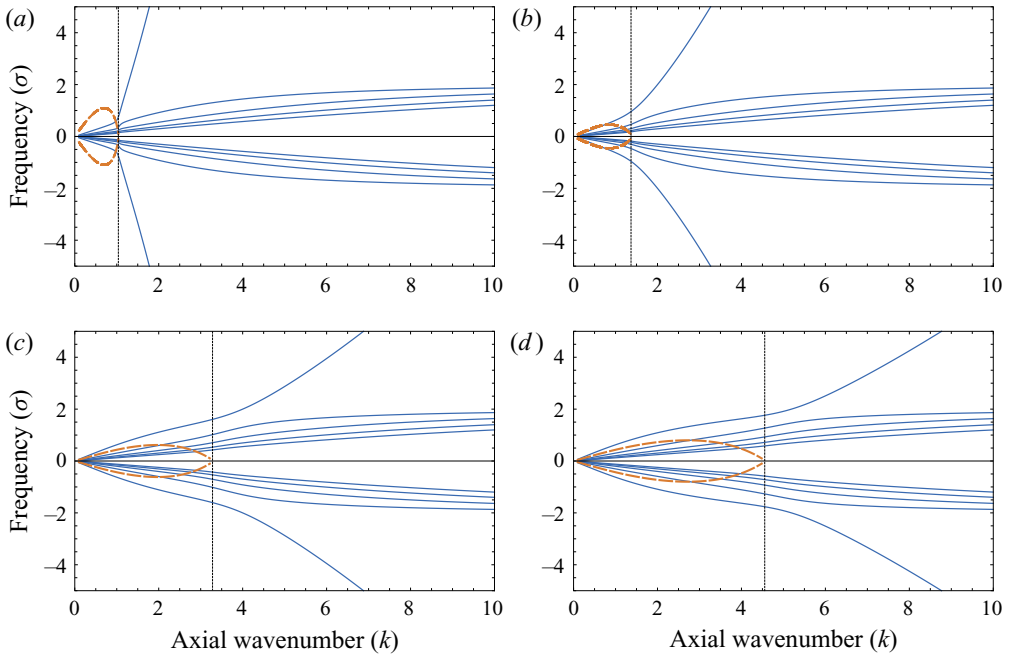

Figure 2. The dispersion curves of the rotating liquid column with varying *We*: (*a*) $We = 0.1$; (*b*) $We = 1$; (*c*) $We = 10$; (*d*) $We = 20$. Blue curves denote neutral modes while dashed orange curves denote growing / decaying modes. A vertical dashed line drawn at $k = \sqrt{1 + We}$ indicates the axial wavenumber beyond which the effects of surface tension on the neutral modes become significant.

of capillary modes (whether neutral or unstable), which are now irrotational. For these modes, the non-dimensional frequency (σ) in (2.1) diverges in the limit of zero rotation. Thus, α reduces to ik and one recovers the Rayleigh–Plateau dispersion relation given in (1.1). In contrast, the Coriolis modes, which remain vortical in the zero-rotation limit, may be regarded as a complete set of stationary vortical perturbations that do not perturb the column free surface. For these modes, the non-dimensional frequency σ remains finite (implying that the dimensional one vanishes as $O(\Omega)$) and, therefore, so does α. The dispersion relation reduces to $We\,\mathrm{J}_0(\alpha)/\mathrm{J}_1(\alpha) = k(k^2 - 1)$, implying that $\mathrm{J}_1(\alpha) = 0$ governs the Coriolis mode frequencies for $We = 0$; this also ensures that the radial velocity vanishes at $r = 1$ (see 3.2*a* in Kubitschek & Weidman (2007*a*)), consistent with the aforementioned requirement of an unperturbed free surface. An analogous limiting scenario prevails for any non-zero n, with the limiting dispersion relation being given by $\sigma - n = (2n\,\mathrm{J}_n(\alpha))/(\alpha \mathrm{J}_n'(\alpha))$; thus, the Coriolis modes, in all cases, reduce to stationary vortical perturbations as $We \to 0$, and are irrelevant to the dynamics of free surface disturbances.

Finally, it needs mentioning that while the growing and decaying modes for the rotating column exist over a wider range of wavenumbers given by $0 < k < \sqrt{1 + We}$, they do not emerge as a result of coalescence of neutral modes, as was the case for the Rayleigh–Plateau problem (where the so-called 'principle of exchange of stability' holds); instead, as evident from the dashed dispersion curves in figures 1 and 2, they arise independently as the stability threshold is crossed. Importantly, since the eigenvalues associated with these modes are purely imaginary, the state of neutral stability is one of rigid rotation, and therefore, as pointed out by Rosenthal (1962), viscosity cannot alter

the threshold. Thus, $We = k^2 - 1$ remains the threshold regardless of the column Reynolds number (which may be defined as $Re = \Omega a^2/\nu$, with ν being the kinematic viscosity).

2.2. *Planar perturbations*

Next, we examine planar perturbations, the inviscid dispersion relation for which was first obtained by Hocking & Michael (1959) and is given by

$$\sigma = n - 1 \pm \sqrt{\frac{(n-1)(n(n+1) - We)}{We}}, \tag{2.3}$$

which is algebraic (quadratic) instead of transcendental, as was the case for axisymmetric perturbations (see (2.1)), and as is also the case for helical perturbations (see (2.6)). The existence of only a pair of planar modes is because the infinite number of Coriolis modes degenerate to $\sigma = n$ for $k \to 0$ in the inviscid limit, see figures 1(*c*) and 4(*a*). For any We, the two planar-wave frequencies are symmetrically distributed about $n - 1$. For small We, they are asymptotically large (of $O(We^{-1/2})$, which corresponds to a dimensional frequency of $\sqrt{\gamma/\rho a^3}$, as expected, and approach each other with increasing We. For $n \geq 2$, the modes coalesce at $\sigma = n - 1$ for $We = n(n+1)$, the inviscid threshold mentioned earlier, and become complex valued for $We > n(n+1)$, implying instability.

Unlike the axisymmetric case, viscosity has a profound effect on the stability of the rotating column to planar perturbations. To see this, let $\Lambda = n(n^2-1)/We - n$ so that the pair of inviscid frequencies above may be written as $\sigma = n - 1 \pm \sqrt{1+\Lambda}$ and the inviscid threshold corresponds to $\Lambda = -1$. For large but finite Re, Hocking (1960) obtained the following expressions for the planar-wave frequencies, corrected for viscous effects, again as the solutions of a quadratic equation:

$$\sigma = n - 1 \pm \sqrt{1+\Lambda} - \frac{\mathrm{i}}{Re}\left(2n(n-1)\frac{-1 \pm \sqrt{1+\Lambda}}{\pm\sqrt{1+\Lambda}}\right). \tag{2.4}$$

Note that the $O(1/Re)$ scaling for the viscous correction, implied by (2.4), is not valid near the inviscid threshold as the expression within brackets diverges for $\Lambda \to -1$. One may nevertheless derive the requirement for viscous instability. This corresponds to σ in (2.4) having a negative imaginary part which in turn translates to $\Lambda = 0$ (bounded away from the aforementioned breakdown value), or $We = n^2 - 1$. This threshold was shown to be applicable for columns of all finite Re (Gillis 1961). Rather counter-intuitively, on one hand, the viscous threshold does not depend on Re, leading to the aforementioned discontinuous jump in the threshold We from $n(n+1)$ to $n^2 - 1$. On the other hand, the viscous threshold for stability is less than the inviscid threshold, implying the destabilizing influence of viscosity. The latter behaviour is attributed to the phase difference between pressure and displacement waves. The two waves are exactly out of phase in the inviscid limit. This is no longer true in presence of viscous effects which allow for a net work done during a single oscillation. The role of viscosity in modifying the phase difference, and thereby inducing exponential growth, is reminiscent of the Miles mechanism that accounts for the growth of wind-driven gravity waves (Miles 1957; Benjamin 1967); although, on account of the rigidly rotating base state, there isn't the complicating effect of a critical layer (Miles 1957) in the present problem.

Figures 3(*a*) and 3(*b*) show that although the stability threshold changes discontinuously for any finite Re, the growth rates in the interval between the inviscid and viscous thresholds ($n^2 - 1 < We < n(n+1)$) scale viscously, and therefore, decrease to zero for

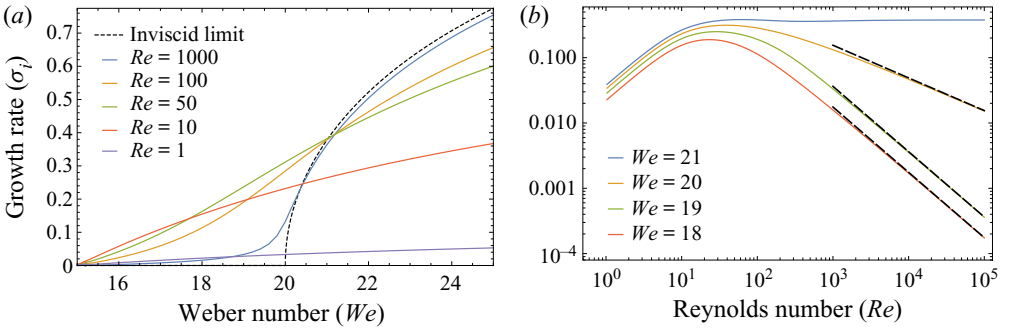

Figure 3. The two figures plot the growth rates of planar perturbations as a function of We and Re for $n = 4$: (a) growth rates versus We for various Re; (b) growth rates versus Re for various We. Note the discontinuous change in the stability criterion from $We = 20$, for the inviscid case (the dotted black curve in (a)) to $We = 15$ for any finite Re. Dashed black lines in (b) denote the large Re asymptotes obtained from the planar viscous dispersion relation due to Hocking (1960).

$Re \to \infty$ (see also the figure in Gillis (1961) and figure 6c in Kubitschek & Weidman (2007a)). For $We \in (n^2 - 1, n(n+1))$, the growth rates scale as Re^{-1}, while remaining $O(1)$ for $We > n(n+1)$. Within a small $O(Re^{-2})$ interval around $We = n(n+1)$, the growth rates exhibit a slower decay of $O(Re^{-1/2})$ for $Re \to \infty$, consistent with the singular role of viscosity in the neighbourhood of the inviscid threshold, implied by (2.4), see figure 3(b). Finally, it is worth mentioning that the viscous dispersion relation is a transcendental one even for planar modes (Hocking 1960). Thus, for any finite Re, there exist an infinite number of planar modes and, importantly, they remain non-degenerate. It may be shown that all but two of these modes (the two being governed by the corrected quadratic derived by Hocking, given by (2.4)) have $\sigma_r \to n\Omega$, with $\sigma_i \sim O(Re^{-1})$ in the limit $Re \to \infty$. The zero Doppler frequency limit ($\sigma_r - n\Omega = 0$) suggests that these remaining modes correspond to the limiting forms of the planar Coriolis modes for large but finite Re. In fact, for any finite Re, the σ_i values for the Coriolis modes form an infinite sequence going asymptotically to $-\infty$ with increasing modal index, this being consistent with the fact that the finer-scaled modes must exhibit progressively greater (viscous) decay rates.

2.3. *Three-dimensional perturbations*

The effect of rotation on three-dimensional perturbations is well understood only in the presence of viscosity. As shown first by Gillis & Kaufman (1962), the necessary and sufficient criterion for the stability of the rotating column in the presence of viscosity is

$$We < k^2 + n^2 - 1. \tag{2.5}$$

It is easily seen that (2.5) reduces to the corresponding criteria for viscous planar and axisymmetric perturbations for $n = 0$ and $k = 0$, respectively. For inviscid stability, however, this criterion has only been shown to be a sufficient one (Pedley 1967). The relevance of the same threshold $We(= k^2 + n^2 - 1)$ in the presence and absence of viscosity is because, as will be seen below, similar to the axisymmetric case, the system is in a state of rigid-body rotation at this We. However, the change from a necessary and sufficient condition in the viscous case to only a sufficient one in the inviscid limit points to the possibly subtle relation between the inviscid and viscous stability scenarios.

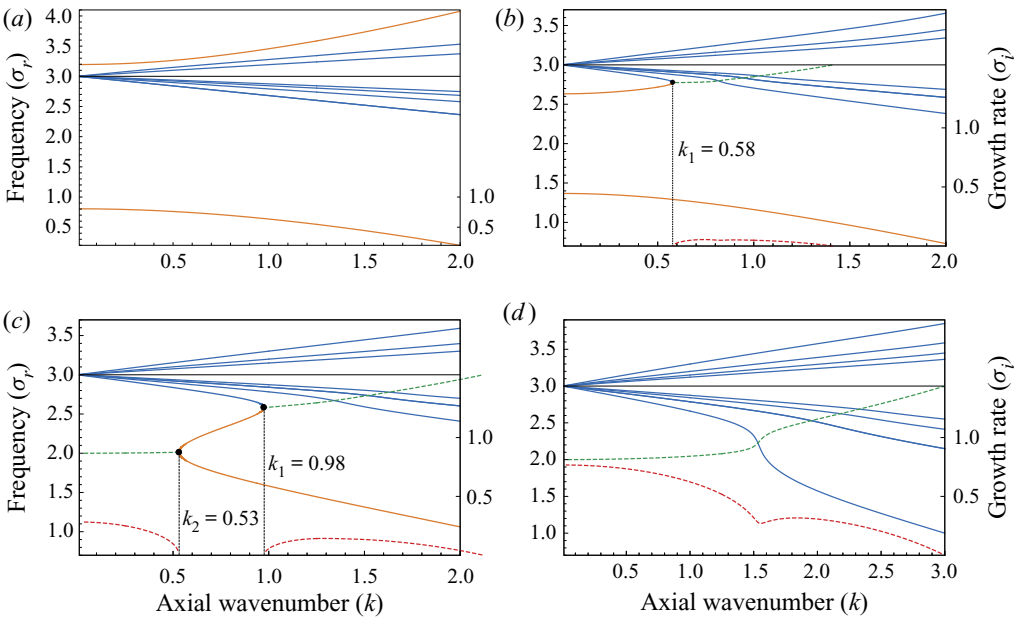

Figure 4. The inviscid dispersion curves corresponding to the different We regimes for $n = 3$: (*a*) $We < n^2 - 1$ ($We = 7$); (*b*) $n^2 - 1 < We < n(n+1)$ ($We = 10$); (*c*) $n(n+1) < We < We_{cusp}$ ($We = 12.5$); (*d*) $We > We_{cusp}$($We = 17$); where $We_{cusp} \approx 16$ for $n = 3$. The neutral Coriolis modes are shown in blue and the neutral capillary modes in orange. The real part of the unstable eigenvalues are shown as dashed green curves while the imaginary parts are shown as dashed red curves.

The dispersion relation for the inviscid rotating column has, in fact, already been given by Weidman *et al.* (1997) as

$$\alpha \frac{\mathrm{J}_{n-1}(\alpha)}{\mathrm{J}_n(\alpha)} - \frac{We\left(4 - (\sigma - n)^2\right)}{We + 1 - n^2 - k^2} - n\left(1 + \frac{2}{(\sigma - n)}\right) = 0, \tag{2.6}$$

where $\alpha = k\sqrt{4/(\sigma - n)^2 - 1}$. It will be shown below that, for a given $n > 1$, the spectrum as governed by (2.6) changes qualitatively with increasing We. This is illustrated in figure 4 which shows four sets of dispersion curves, for $n = 3$, each corresponding to a different regime.

The first regime, $We < n^2 - 1$ ($= 8$ for $n = 3$), corresponds to the case where the rotating column is stable since We is below the aforementioned viscous threshold; the dispersion curves for this We are shown in figure 4(*a*). Similar to the axisymmetric case (see figure 1), the spectrum consists of a pair of capillary modes (orange) and an infinite hierarchy of Coriolis modes (blue), the first few of which are shown in the figure. As We is increased, the capillary branches move towards each other with the upper branch moving down towards smaller σ. This is in accordance with (2.3) above, which shows that the two capillary branch frequencies in the planar limit ($k = 0$) approach $n - 1$ with We approaching the inviscid threshold. Since the Coriolis modes degenerate to $\sigma = n$ in the planar limit ($k = 0$), this motion of the upper capillary branch would seem to cause it to cross the Coriolis modes with increasing We. The coalescences of the retrograde capillary mode with the retrograde Coriolis dispersion curves, that result after the crossing, would then appear to lead to the emergence of unstable modes at higher We. Note that such a scenario was not possible in the axisymmetric case, where the frequency in the limit $k \to 0$

was identically zero regardless of the particular dispersion curve (capillary or Coriolis) or We, see figure 2.

The second regime, $n^2 - 1 < We < n(n+1)$, is where, as already seen for $k = 0$, the column is unstable (to planar perturbations) only in the presence of viscosity. As shown in figure 4(*b*), the upper capillary branch appears to have moved below the line corresponding to $\sigma = n$, and now suffers a coalescence with the lowermost Coriolis branch at $k_1 \approx 0.58$. This coalescence is accompanied by the pair of eigenvalues becoming complex-valued for larger k, implying instability. The instability continues until the column approaches a state of rigid rotation, corresponding to $We = k^2 + n^2 - 1$, and the corresponding wavenumber is therefore given by $\sqrt{We - n^2 + 1}$. Thus, the lone interval of instability in this regime is given by $k_1 < k < \sqrt{We - n^2 + 1}$ with the upper limit being $\sqrt{2}$ for $n = 3$ and the chosen We in figure 4(*b*).

At $We = n(n+1)$, the pair of capillary branches coalesce at $k = 0$, the corresponding value of σ being $(n-1)$, as predicted by (2.3). Thus, for We larger than $n(n+1)$, the eigenspectrum exhibits two coalescences, resulting in the unstable intervals $0 < k < k_2$ and $k_1 < k < \sqrt{We - n^2 + 1}$ (for the values chosen in figure 4(*c*), $k_1 \approx 0.98$ and $k_2 \approx 0.53$). The first interval corresponds to the unstable mode that results from the coalesced pair of capillary modes, and its lower limit ($k_2 = 0$ at $We = n(n+1)$) denotes the onset of inviscid instability to planar perturbations. The two coalescences lead to an intervening stable interval given by $k_2 < k < k_1$ (figure 4*c*). As a result, the composite dispersion curve that describes the neutral mode is now a combination of portions of the original Coriolis and capillary branches, and has a hysteretic character, as evident from the dispersion curve bending back in the aforementioned stable interval. Although, strictly speaking, the participating Coriolis and capillary modes lose their identity, and only a composite curve remains, an intuitive association of its parts with the original curves is clear. We, therefore, continue to colour portions of the composite curve based on the underlying 'parent' curves. With increasing We, k_1 and k_2 approach each other and the hysteretic region shrinks and eventually vanishes. The critical We where hysteresis vanishes is termed We_{cusp}; as explained below, this is because the disappearance of the hysteretic region is marked by a cusp in the We–k plane. The third regime can then be defined as $n(n+1) < We < We_{cusp}$. For $n = 3$, $We_{cusp} \approx 16$ (see figure 7*b*).

The fourth regime corresponds to $We > We_{cusp}$ when the fold in the dispersion curve and, thence, the intermediate stable wavenumber interval vanishes. There is now only a single unstable interval corresponding to $0 < k < \sqrt{We - n^2 + 1}$ (figure 4*d*), consistent with the aforementioned viscous criterion.

The results presented above agree quantitatively with the restricted observations of Weidman *et al.* (1997) who obtained the (inviscid) growth rates for $n = 1, 2$ and 3, as a function of k, for $We = 10$. Consider figure 5(*a*) in Weidman *et al.* (1997), where the authors present growth rates for $n = 2$ and 3. Since $10 > We_{cusp}$ for $n = 2$, the growth rates correspond to the fourth regime according to the classification above. Nevertheless, the local minimum seen in the growth rate curve for $n = 2$ (akin to the dotted red curves in figures 4*d* and 5*d*) is reminiscent of the hysteresis that occurs at a smaller We. The growth-rate curve for $n = 3$ presented in the same figure matches quantitatively with the dotted red curve in figure 4(*b*). Since $n(n+1) < 10 < We_{cusp}$ for $n = 3$, this growth-rate behaviour corresponding to the second regime described above. Their observations for $n = 1$ can be similarly understood based on the discussion presented in the Appendix. Thus, while our results are consistent with the earlier findings in Weidman *et al.* (1997), our focus on the entire inviscid eigenspectrum allows us to move beyond growth rates

calculations for specific We values, and thereby, infer the implications of the growth-rate behaviour on the relation between the inviscid and viscous stability criteria.

The general behaviour of the dispersion curves with increasing We, highlighted above, holds for all n values greater than unity. Figure 5 shows an analogous behaviour of the eigenspectrum for $n = 4$ with $We_{cusp} \approx 25$. The dispersion curves, such as those in figures 4 and 5, may be stacked upon one another, along the We axis, so as to demarcate the regions of inviscid stability in the We–k plane for each n. Figure 6 shows schematically how this may be achieved (the unstable wavenumber ranges have been omitted for clarity). With varying We, projections of the pair of folding points associated with each hysteretic dispersion curve (the black dots in figures 4*c*, 5*c* and 6), that mark the intermediate stable interval in the σ–k plane, yield the two branches of a stable island in the We–k plane. The picture is that of a cusp catastrophe (Zeeman 1976), implying that the aforementioned pair of branches terminates in a cusp. The points of coalescence between a capillary mode and the lowest retrograde Coriolis mode (figures 4*b* and 5*b*) yield the upper branch of the stable island, while those between the two capillary modes (figures 4*c* and 5*c*) yield the lower branch. The cusp-shaped islands of inviscid stability in the We–k plane, for $n = 2, 3, 4$ and 5, are shown in figure 7. While closed form expressions for the boundaries of these islands are not available, one may nevertheless obtain their small-k approximations. For the lower branch, one has $\sigma \to n - 1$ for $k \to 0$; the resulting limiting form of the dispersion relation gives the required approximation as $k \sim \sqrt{((n^2 - 1)/n(n + 1))(We - n(n + 1))}$. For the upper branch, however, $(\sigma - n)/k$ remains $O(1)$ as $k \to 0$. Since this remains true for all of the Coriolis mode branches, the upper branch asymptote is obtained by exploiting the fact that the slope of the hysteretic dispersion curve diverges at the turning points. Thus, simultaneously solving (2.6) with $d\sigma/dk \to \infty$ for $k \to 0$ yields the small-k approximation for the upper branch. These approximations have been shown as dashed black curves in figure 7, where they are seen to compare well with the numerically determined island boundaries well beyond the rigorous interval of validity ($k \ll 1$). While one expects the We–k plane to remain similar in form for $n > 5$, the scenario for $n = 1$ is essentially different, and is analysed in the Appendix. In this case, there exists only one stable island that extends to infinity along the We axis. The exceptional behaviour is not entirely unexpected, given that the limit $k \to 0$ is a singular one – $n = 1$ corresponds to a mere translation of the rotating column in the planar limit.

The discussion along with the preceding figures establish the following behaviour. With increasing We, the upper capillary branch moves down to lower frequencies, appearing to cross the zero-Doppler-frequency line $\sigma = n$ in the process and, thereafter, undergoes a pair of coalescences (one with the lowest Coriolis mode, and the other with the lower capillary branch). These coalescences lead to intermediate unstable ranges of wavenumbers which, with varying We, trace out a stable island in the We–k plane (see figure 7). There are two subtle aspects with regard to this general behaviour that need amplification, however. The first is that the upper capillary branch does not, in fact, end up crossing $\sigma = n$ (hence, the usage 'appears to' in all the instances above). Instead, as shown in figure 8, at $We = n^2 - 1$, when the zero-k frequency of this branch equals $\sigma = n$ (figure 8*d*), the capillary branch stops moving downward as a whole; instead, a new discrete mode emanates from $\sigma = n$, and continues down into the retrograde frequency range with further increase in We (figures 8*e* and 8*f*). Further, even as the upper capillary branch descends towards $\sigma = n$, for We just below $n^2 - 1$, it never crosses the lower cograde Coriolis branches. These 'avoided crossings' are illustrated via suitably magnified views in figure 8(*a–c*), and arise from the Krein signature criterion, required for unstable

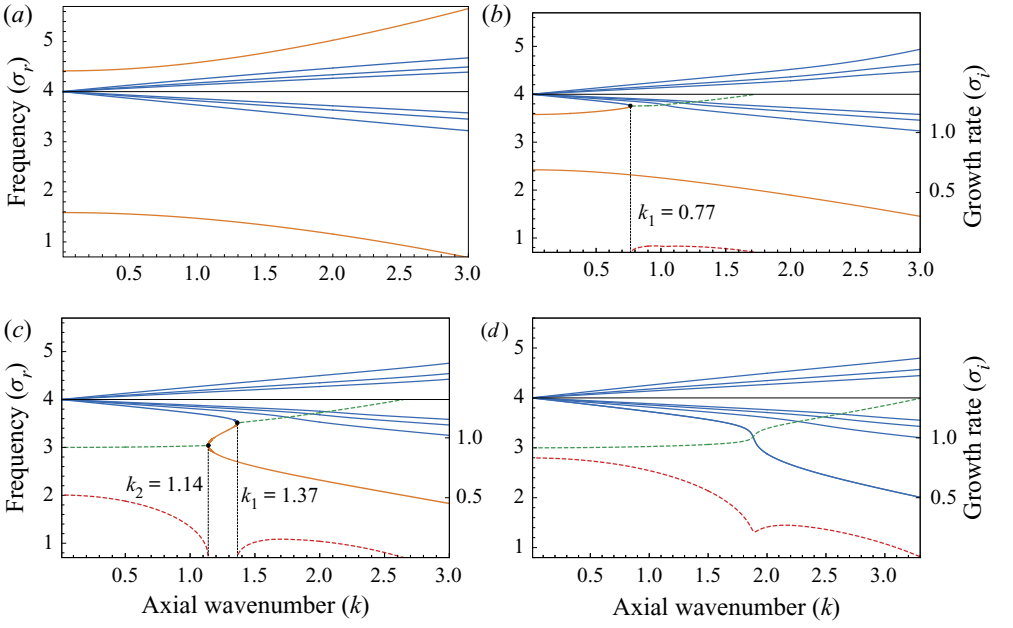

Figure 5. The inviscid dispersion curves corresponding to the different *We*-regimes for $n = 4$: (*a*) $We < n^2 - 1$ ($We = 12$); (*b*) $n^2 - 1 < We < n(n+1)$ ($We = 18$), (*c*) $n(n+1) < We < We_{cusp}$ ($We = 22$); (*d*) $We > We_{cusp}$ ($We = 26$); where $We_{cusp} \approx 25.5$ for $n = 4$. The neutral Coriolis modes are shown in blue and the neutral capillary modes in orange. The real part of the unstable eigenvalues are shown as dashed green curves while the imaginary parts are shown as dashed red curves.

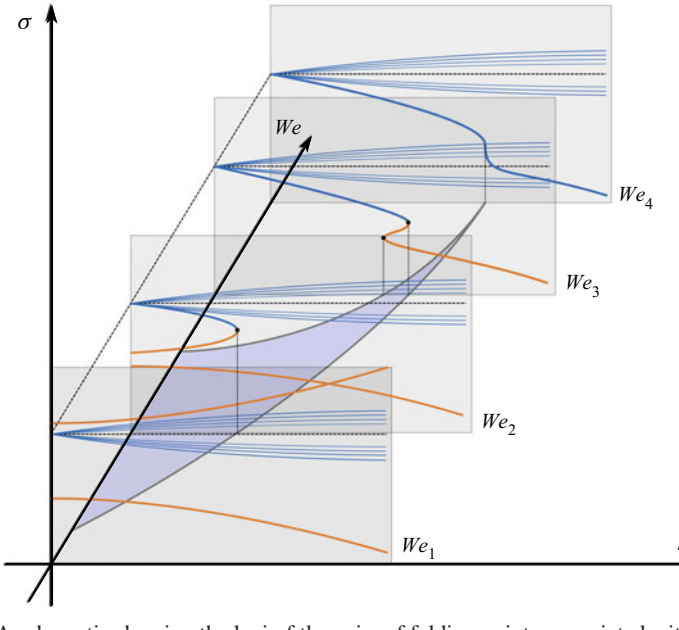

Figure 6. A schematic showing the loci of the pairs of folding points, associated with the hysteretic dispersion curves, which leads to the inviscidly stable island in the *We*–*k* plane.

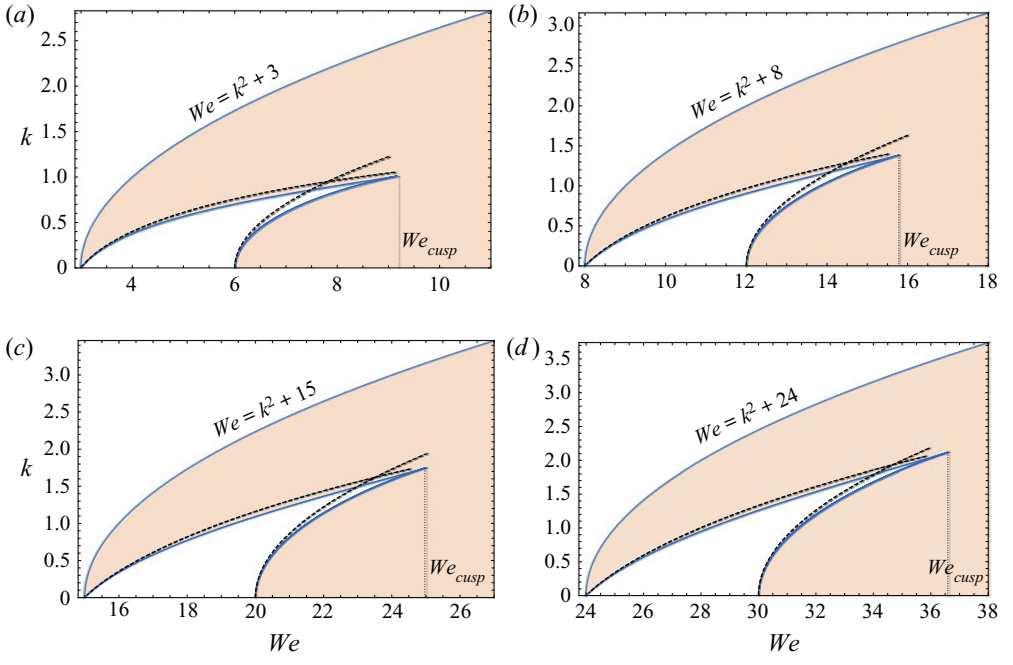

Figure 7. Depiction of the stable islands in the *We*–*k* plane for (*a*) $n = 2$, (*b*) $n = 3$, (*c*) $n = 4$ and (*d*) $n = 5$. Blue curves denote both, the outer boundary ($We = n^2 + k^2 - 1$) and the numerically obtained boundaries of the inviscidly stable island within; the shaded region between these boundaries denotes the inviscidly unstable region. The dashed black curves denote the small-k asymptotes for the island boundaries; the lower branch asymptote is $k \sim \sqrt{((n^2-1)/n(n+1))(We - n(n+1))}$ and that for the upper branch is obtained by simultaneously solving $\mathrm{d}\sigma/\mathrm{d}k = \infty$ with (2.6) for small k.

coalescences between different modal branches, not being satisfied for cograde modes (Mackay & Meiss 1987; Fukumoto 2003; Chernyavsky, Kevrekidis & Pelinovsky 2018).

The second subtle aspect is related to the retrograde mode above that bifurcates from the cograde capillary mode at $\sigma = n$. In moving further down towards $\sigma = n - 1$ with increasing *We* (at which point this mode undergoes a coalescence with the lower capillary branch, leading to an unstable wavenumber interval $(0, k_2)$, as illustrated in figures 4*c* and 5*c*), the mode must end up crossing an infinite number of Coriolis mode branches, in turn implying the possibility of an infinite hierarchy of coalescences, instead of just the single one with the lowermost (retrograde) Coriolis branch shown in figures 4(*b*) and 5(*b*). Note that the infinite number of crossings must occur in the neighbourhood of $\sigma = n$ which, from (2.3), corresponds to $We = n^2 - 1$. Therefore, one may verify the existence of such a hierarchy of crossings by checking for the occurrence of coalescences in the eigenspectra in the vicinity of $We = n^2 - 1$. It turns out that all of the crossings of the aforementioned retrograde mode with the retrograde Coriolis modes lead to coalescences and, thence, hysteretic dispersion curves with intermediate unstable k-intervals. The number of such hysteretic curves increases rapidly as *We* approaches $n^2 - 1$ from above. Figure 9 depicts the increasing number of hysteretic dispersion curves that result for $n = 3$ for $We \to 8^+$; there is one coalescence for $We = 8.5$, three for $We = 8.2$ and four for $We = 8.1$, besides the original coalescence between the new retrograde mode and the lowest Coriolis mode, with successive coalescences occurring at progressively smaller k. Figure 10 provides a magnified view of the ensemble of dispersion curves for

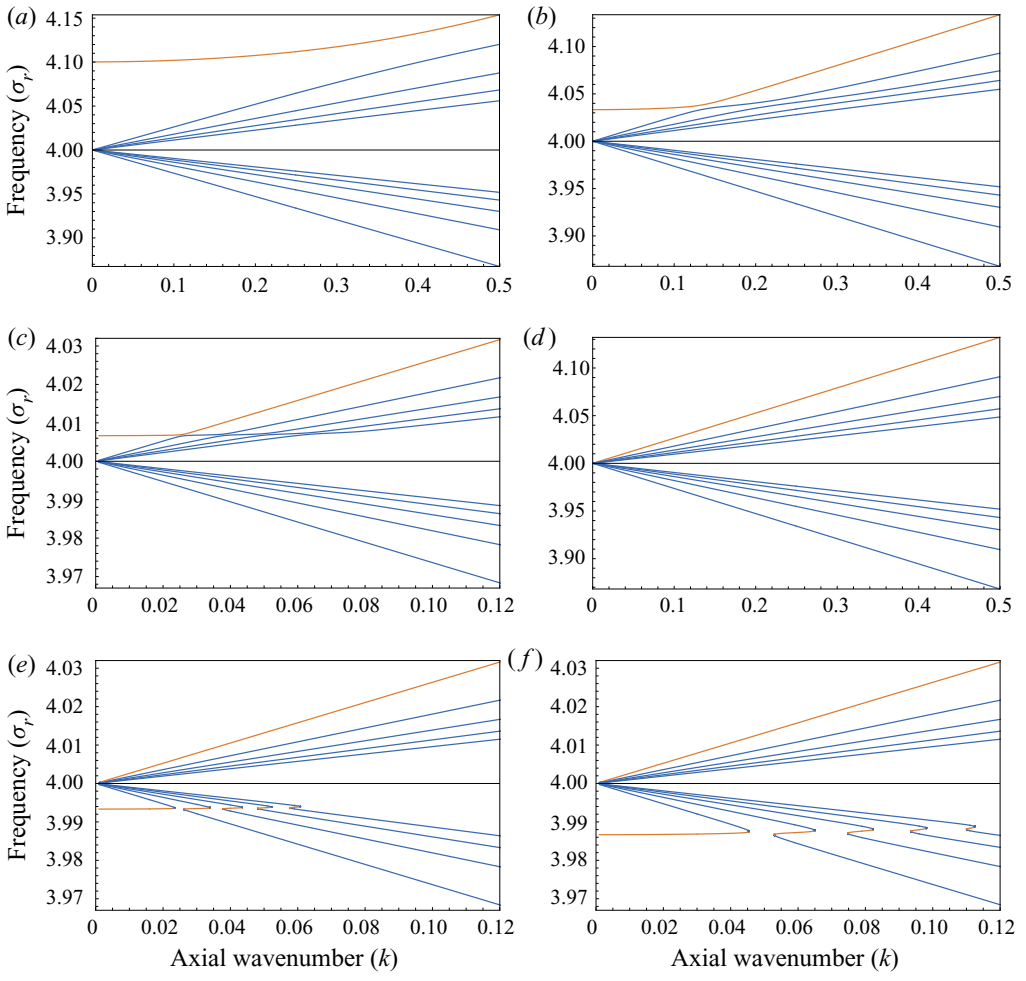

Figure 8. Dispersion curves (σ versus k) for $n = 4$ and We close to $n^2 - 1$: (*a*) $We = 14.25$; (*b*) $We = 14.75$; (*c*) $We = 14.95$; (*d*) $We = 15$; (*e*) $We = 15.05$; (*f*) $We = 15.1$. At $We = n^2 - 1$ the capillary mode splits into two and yields a new retrograde mode (also shown in orange) which subsequently undergoes an infinite sequence of coalescences with the retrograde Coriolis modes for higher We.

$We = 8.1$, emphasizing the rapid oscillations in the growth rate owing to the multiple closely spaced intervals of stability. Similar to figure 7, each of these hysteretic intervals marks out a stable island in the We–k plane. Therefore, in the inviscid limit, there appears to be an infinite hierarchy of neutrally stable islands (each of these associated with a cusp catastrophe, or a fold in the three-dimensional surface characterizing the We–k–σ relationship as illustrated in figure 6) enclosed within the viscously unstable region given by $We > n^2 + k^2 - 1$. This infinite hierarchy of inviscidly stable islands only appears above, and not below, the viscous threshold since, as already pointed out, the cograde modes exhibit avoided collisions (figure 8*a*–*c*), while the retrograde modes coalesce, yielding complex eigenvalues, consistent with their respective Krein signatures. The higher-order stable islands are much smaller than the leading one, and decrease in size rapidly, eventually going asymptotically to the limit point $(We, k) = (n^2 - 1, 0)$. The resulting picture in the We–k plane is illustrated in figure 11 for $n = 2, 3, 4$ and 5.

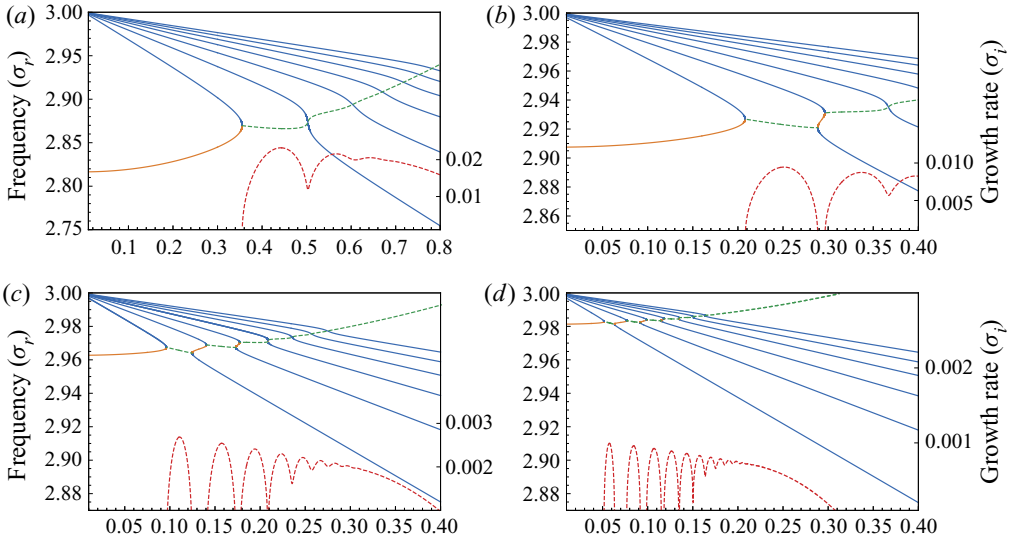

Figure 9. An increasing number of retrograde dispersion curves exhibit a hysteretic character for $We \to (n^2-1)^+$; the figures show this behaviour for $n = 3$. (*a*) A single coalescence between a capillary and a Coriolis mode: $We = 9$. (*b*) The capillary-Coriolis coalescence plus a single hysteretic dispersion curve: $We = 8.5$. (*c*) The capillary-Coriolis coalescence plus three hysteretic dispersion curves: $We = 8.2$. (*d*) The capillary-Coriolis coalescence plus four hysteretic dispersion curves: $We = 8.1$.

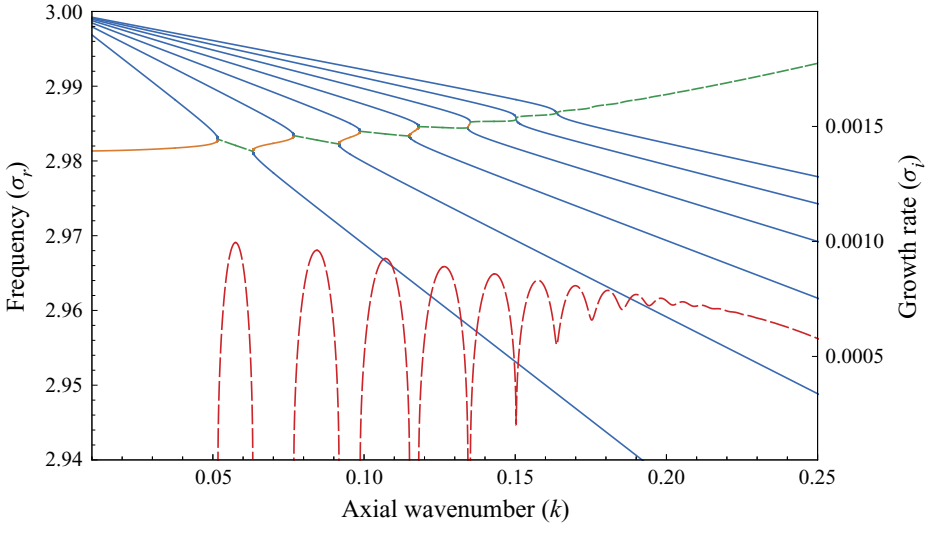

Figure 10. A magnified view of figure 9(*d*): $We = 8.1$; $n = 3$. Note the multiple hysteretic dispersion curves (four, besides the original) and corresponding oscillations in the growth rate.

Each of the panels shows five leading satellite islands besides the main island, of what is likely an infinite hierarchy. As implied by figure 10, a consequence of this infinite hierarchy is a rapid alternation of regions of stability and instability as one increases k for a fixed We and, thence, a rapidly fluctuating growth rate with changing k.

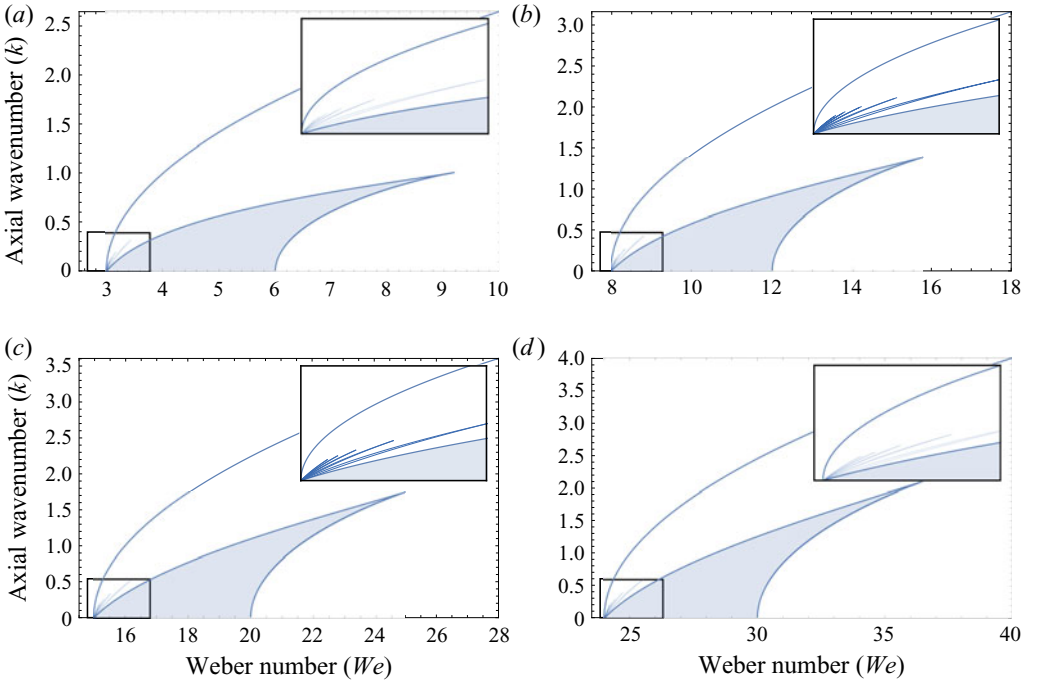

Figure 11. The main and satellite islands of inviscid stability, in the We–k plane, for (*a*) $n = 2$, (*b*) $n = 3$, (*c*) $n = 4$ and (*d*) $n = 5$. Magnified views, of five of the infinite hierarchy of satellite islands, appear in the insets.

3. Conclusion

In this paper, we have analysed the inviscid stability of a rotating liquid column as a function of We, and the axial and azimuthal wavenumbers (k and n) of the imposed perturbation, with a focus on the entire eigenspectrum that includes a pair of capillary modes and an infinite hierarchy of Coriolis modes in the general case. While it is known that a viscous rotating column becomes unstable if and only if $We > k^2 + n^2 - 1$, consideration of the full eigenspectrum highlights the intricate nature of the inviscidly unstable region in the We–k plane. The intricacy arises from the likelihood of an infinite hierarchy of coalescences between pairs of dispersion curves in the neighbourhood of the planar viscous threshold ($We = n^2 - 1$). As illustrated in figure 11, these coalescences appear to lead to an infinite hierarchy of inviscidly stable islands within the viscously unstable region ($We > n^2 + k^2 - 1$) in the We–k plane; each of these islands corresponds to a fold in the We–k–σ surface in three dimensions (see figure 6). The existence of these islands explains why $We < n^2 + k^2 - 1$ only serves as a sufficient condition for stability in the inviscid limit (Pedley 1967); evidently, one can be stable even when $We > n^2 + k^2 - 1$, provided one is inside any of these islands. Thus, the necessary and sufficient condition for inviscid instability would require $We > n^2 + k^2 - 1$ and, in addition, that the (We, k, n) triplet chosen lies outside the inviscid islands identified in figure 11. It is not possible to provide a precise expression for this criterion since, as already pointed out, closed form expressions for the island boundaries are not known; although, the small-k asymptotes appear to serve as useful approximations especially for the larger n values (see figure 7). Interestingly, it has been shown in the appendix of Weidman *et al.* (1997) that one may again obtain only a sufficient condition for inviscid stability for the analogous

two-fluid system. Thus, for a configuration consisting of a central column of a denser liquid and an annular domain of a lighter one, both being in a state of rigid-body rotation, the sufficient condition for inviscid stability becomes

$$We_1 - We_2 < k^2 + n^2 - 1, \tag{3.1}$$

which is the natural generalization of the single-fluid criterion encountered earlier, and where We_1 and We_2 are now the Weber numbers based on the inner and outer fluid densities. Although the viscous problem and, therefore, the viscous stability criterion for the two-fluid system problem has not yet been examined, the discussion presented here suggests an analogous relationship between the viscous and inviscid criteria.

The discovery of an infinite hierarchy of inviscidly stable islands in the *We*–*k* plane also has implications for viscous stability for large but finite *Re*. As shown in figure 10, for the case $n = 3$ and $We = 8.1$, the inviscid growth rate oscillates rapidly between zero and order-unity values, with the oscillations becoming increasingly dense and rapid for $We \to 8^+$ (the value of $n^2 - 1$ for $n = 3$); interestingly, although the growth rates decrease for $We \to (n^2 - 1)^+$, as expected, the amplitude of the oscillations, for a fixed *We*, does not appear to decay with increasing order of the modal coalescence, the order here referring to the modal index of the (retrograde) Coriolis mode involved in the particular coalescence. Now, for large but finite *Re*, one expects only a finite number of oscillations regardless of the proximity of *We* to $n^2 - 1$. This is because, as mentioned in § 2.2, the viscous decay rates for planar perturbations can attain arbitrarily high values for large enough modal indices, owing to the vanishingly small radial scale associated with the eigenfunction. Thus, for finite *Re*, however large, one expects the (inviscid) growth rate associated with modal coalescences above a certain threshold order to be overwhelmed by viscous decay. Nevertheless, for an *Re* large enough that the spacings between adjacent islands is greater than $O(Re^{-2})$, one expects rapid oscillations in the growth rate between order-unity values between the islands, and $O(Re^{-1})$ values within them. While the *Re* values required to see substantial growth-rate oscillations requires a full viscous calculation, it does appear that the *Re* values involved might be very large. In contrast, experiments on the rotating liquid column have only accessed a maximum *Re* of $O(10)$, see Kubitschek & Weidman (2008).

The question of *Re* being large enough for one to be able to observe the aforementioned oscillations in the (viscous) growth rate leads us to the astrophysical analogue of the configuration examined thus far – that of a rotating self-gravitating fluid column, which may be likened to a large-scale filamentary structure; such structures appear to have a ubiquitous presence in the interstellar medium and are regarded as playing an important role in the star formation process (André 2017). Chandrasekhar and Fermi performed one of the earliest studies on the stability of a self-gravitating columnar configuration (see Chandrasekhar & Fermi 1953; Chandrasekhar & Lebovitz 1964). Their calculations were done in the incompressible limit when the column has a uniform density and a finite radius, and revealed an axisymmetric instability. Analogous to the Rayleigh–Plateau instability of the liquid column, the axisymmetrically deformed fluid (gas) column has a lower gravitational potential energy than the original columnar configuration for sufficiently long-wavelength perturbations and is therefore unstable to all axisymmetric perturbations with wavelengths longer than 1.0668 times the column radius (Chandrasekhar 1981, p. 519). Subsequently, Ostriker extended the analysis of Chandrasekhar & Fermi (1953) to a compressible columnar configuration, evaluating the base-state density profiles using a polytropic equation of state for different values of the polytropic index (Ostriker 1964*a*). Compressibility leads to an inhomogeneous base state with a finite radial extent, the isothermal case alone being an exception. Next, Ostriker (1964*b*) analysed the effects of compressible perturbations on a homogeneous finite-radius

cylinder (a solution of the incompressible equations). Later analyses include the stability calculations of Stodólkiewicz (1963) and Nagasawa (1987) for the aforementioned isothermal configuration, and those have again shown axisymmetric disturbances alone to be unstable. On account of filamentary molecular clouds being good representations of spiral galactic arms, and the implications of instability for formation of dense prestellar cores, stability analyses of self-gravitation columnar configurations with or without magnetic fields continue to garner attention (McKee & Ostriker 2007; Breysse, Kamionkowski & Benson 2014; Motiei, Hosseinirad & Abbassi 2021).

Rotation is ubiquitous in self-gravitating filaments, and Hansen, Aizenman & Ross (1976) were one of the first to examine the equilibrium and stability of an isothermal and uniformly rotating cylinder. The inclusion of rotation, and the resulting conflicting effects of rotation and self-gravitation on density stratification, introduces an unusual feature into the equilibrium state – that of a (spatially) damped oscillatory density profile. Hansen *et al.* (1976) analysed the stability of such rotating base states (of a finite radius) to two-dimensional disturbances, and found that rotation renders cylinders, exceeding a critical size, unstable to non-axisymmetric disturbances. Freundlich, Jog & Combes (2014) have recently studied a polytropic rotating cylinder within the framework of a local stability analysis. More recently, Sadhukhan, Mondal & Chakraborty (2016) have extended the local stability analysis to polytropic rotating cylinders, with the addition of a magnetic field, and observe that the background rotation acts to reduce the unstable growth rates. Thus, there exist instances in the literature of rotation having conflicting roles – in terms of both stabilizing and destabilizing self-gravitating masses. To comprehensively understand the role that rotation plays in the stability of filamentary molecular clouds, there is an imminent need for a global three-dimensional stability analysis of rotating polytropic columnar configurations. In this concluding section, however, we only look at the limiting case of an incompressible cylinder – the rotating version of Chandrasekhar and Fermi's seminal study referenced above. This is because our focus here is to primarily draw an analogy between the cohesive forces of surface tension and gravitation; we show below that a rotating self-gravitating incompressible fluid column exhibits an infinite hierarchy of cusp catastrophes analogous to the rotating liquid column above. Although beyond the scope of the present calculation, and despite the known singular role of compressibility (Ostriker 1964*b*), we expect our findings to continue to be relevant for compressible self-gravitating columns.

A linear stability analysis of a self-gravitating cylinder, in a state of rigid-body rotation, readily furnishes the following dispersion relation:

$$\alpha\frac{\mathrm{J}_{n-1}(\alpha)}{\mathrm{J}_n(\alpha)}-\frac{\dfrac{\Omega^2}{2\pi\rho G}(4-(\sigma-n)^2)}{\dfrac{\Omega^2}{2\pi\rho G}-(1-2\mathrm{K}_n(k)\mathrm{I}_n(k))}-n\left(1+\frac{2}{(\sigma-n)}\right)=0, \tag{3.2}$$

where $\Omega^2/2\pi\rho G$ is the analogue of the Weber number for the self-gravitating case, in measuring the relative importance of gravitational and centrifugal forces, G being the gravitational constant. Let us now define

$$We_G = f(n,k)\,\frac{\Omega^2}{2\pi\rho G}, \tag{3.3}$$

where $f(n,k)=(k^2+n^2-1)/(1-2\mathrm{I}_n(k)\mathrm{K}_n(k))$, so that we have, in terms of We_G, a dispersion relation identical to that in (2.6). Since $f(n,k)$ is a monotonically increasing

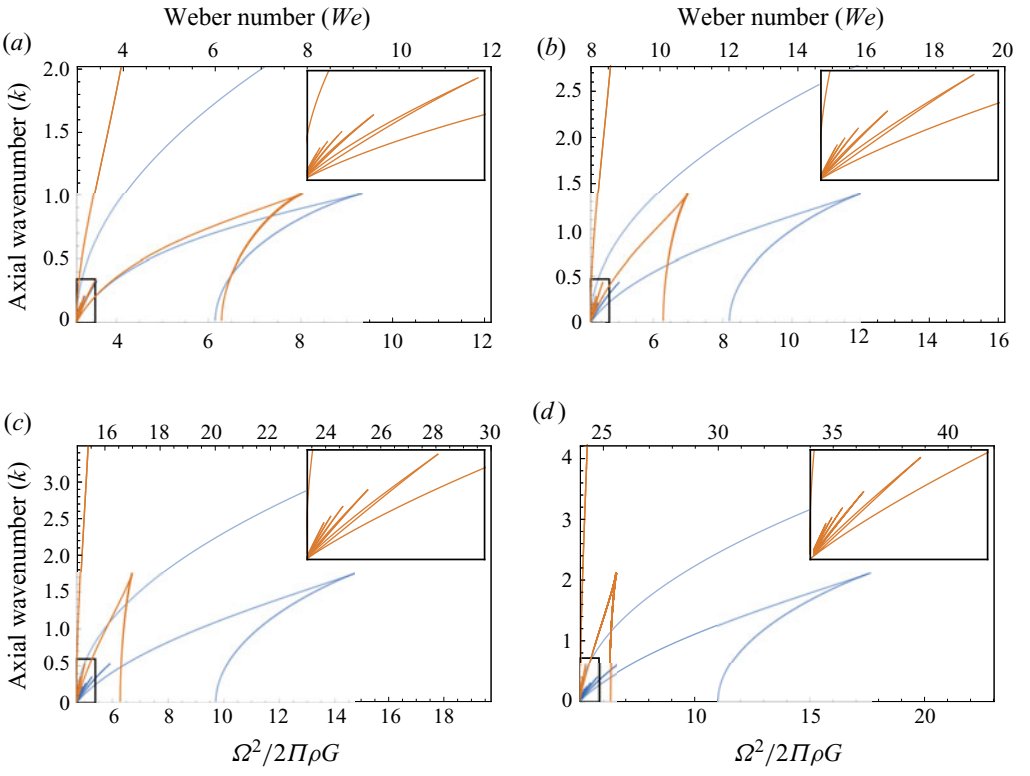

Figure 12. Comparison of the inviscidly stable islands for the surface-tension (blue) and self-gravitating (orange) cases for (*a*) $n = 2$, (*b*) $n = 3$, (*c*) $n = 4$ and (*d*) $n = 5$. The insets in each figure show magnified views of the first five satellite islands for the self-gravitating column.

function of k for a given n, one has a unique value of $\Omega^2/2\pi\rho G$ for every We_G. The $\Omega^2/2\pi\rho G - k$ plane will then be topologically equivalent to the We_G–k plane and, thence, to the We–k plane of the rotating liquid column seen earlier. The resulting infinite hierarchy of cusp catastrophes for the rotating self-gravitating fluid column, and its comparison with the hierarchy already seen above, for the rotating liquid column (with surface tension), is shown in figure 12.

Going beyond the paradigm of Newtonian gravitation, it is worth mentioning that the efforts of Cardoso & Dias (2006) and Caldarelli *et al.* (2009) who have pointed out intriguing similarities between dynamics of black holes and fluid droplets, are again based on the similarities between surface tension and self-gravitation. The authors demonstrate that several aspects of the Gregory–Laflamme instability of black strings can be mapped onto the Rayleigh–Plateau instability of a fluid cylinder. Based on the analogy between rotating liquid drops and rotating black holes, the authors further propose an instability of ultraspinning black holes and suggest inclusion of rotation as a possible direction for further investigation. Although a direct analogy does not hold in this case owing to, for instance, a dependence of the surface tension of a black hole on rotation, the results obtained here nevertheless point to intriguing stability characteristics that might emerge from consideration of more detailed models of rotating self-gravitating astrophysical objects.

As a final note, our findings here apply to a rotating column of a circular cross-section. If there is a departure from circularity, for instance, due to an imposed straining flow,

then additional instability mechanisms come into play. Based on the known example of a strained vortex column (see Moore & Saffman 1975; Tsai & Widnall 1976), there arises the possibility of an instability due to a parametric resonance between eigenmodes with different azimuthal wavenumbers; this, as opposed to an instability from the coalescence of two modes of a given azimuthal wavenumber, as is the case analysed here.

Funding. The majority of this work took place at JNCASR, Bangalore and the funding support from the institute is gratefully acknowledged.

Declaration of interests. The authors report no conflict of interest.

Author ORCIDs.
Pulkit Dubey https://orcid.org/0000-0001-8181-2083;
Anubhab Roy https://orcid.org/0000-0002-0049-2653;
Ganesh Subramanian https://orcid.org/0000-0003-4314-3602.

Appendix. Stability criteria for $n = 1$

For planar perturbations with $n = 1$, one sees from (2.3) that σ vanishes identically for all non-zero *We*. Therefore, the inviscid threshold, $We = n(n + 1)$, is of no relevance in this case, and there can be no analogue of the different *We*-regimes that exist for $n \geq 2$ (see figure 4*a–d*). As already stated in the main text, this is expected since a planar perturbation for $n = 1$ corresponds to a mere translational displacement. Further, for $n \geq 2$, the pair of planar frequencies, corresponding to the two capillary branches, are widely separated, and symmetrically distributed approximately $\sigma = n - 1$, for small *We*. The motion of the upper capillary branch down towards $\sigma = n$, with increasing *We*, and the subsequent birthing of a new retrograde mode at $\sigma = n$, is essential for the infinite hierarchy of coalescences in the $\sigma - k$ plane and, thence, for the infinite hierarchy of inviscidly stable islands in the *We*–*k* plane. In contrast, for $n = 1$, $\sigma = 0$ is a double root of the governing quadratic. Thus, a second mode emanates from $\sigma = 0$, with increasing k, in addition to the retrograde capillary mode, and may be likened to the retrograde mode above, for $n \geq 2$, that undergoes coalescences with the Coriolis modes. But, for $n = 1$, this mode is already below the infinite hierarchy of retrograde Coriolis modes even at the smallest *We* (see figure 13*a*, below), and one may only expect a merger with the lowest member of the Coriolis hierarchy. As a result, one expects a leading stable island, but no satellite islands, in the *We*–*k* plane.

In fact, the nature of the dispersion curves for $n = 1$ does not change qualitatively with increasing *We*. One observes a single coalescence and, thence, a single unstable interval bounded away from $k = 0$, for any finite *We*. Figure 13(*a–d*) confirms this behaviour for *We* ranging from 1 to 10. As $We = 10$ is significantly greater than the hypothetical threshold ($n(n + 1) = 2$), we do not expect this picture to alter for greater *We* values and the resulting stable island in the *We*–*k* plane would thus extend to infinity (figure 13*e*). This, once again, points to the absence of distinct *We* regimes observed for $n \geq 2$. The growth rate and range of unstable wavenumbers shown in figure 13(*d*) are consistent with figure 4 of Weidman *et al.* (1997). Finally, from the growth rate perspective, the $n = 1$ mode remains subdominant for all *Re* greater than 1.166 (approximately). As shown by Kubitschek & Weidman (2007*a*) the azimuthal wavenumber of the dominant perturbation jumps from $n = 0$ to $n = 2$ beyond $Re \approx 1.166$, and then to higher n values with increasing *We*. Thus, the anomalous behaviour of $n = 1$ is less important in the limit of large *Re* as, for instance, in the astrophysical context above.

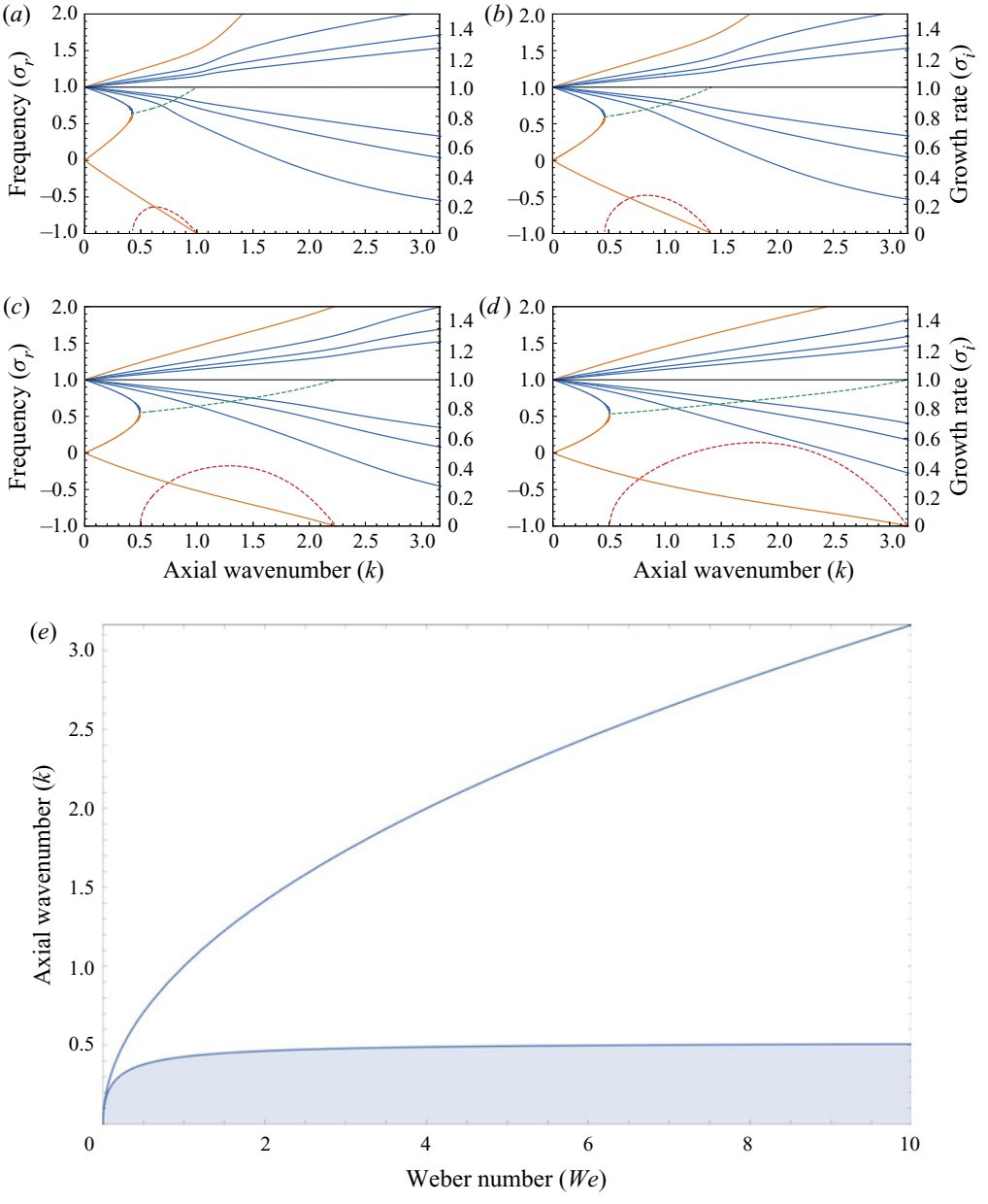

Figure 13. Dispersion curves for $n = 1$ (*a–d*); the solid blue curves indicate the Coriolis modes, the solid orange curves indicate the capillary modes and the dashed curves indicate real (red) and imaginary (green) parts of the unstable modes. Panel (*e*) depicts the stable island generated as a result of coalescence of the lowest Coriolis mode and the retrograde capillary mode. Here (*a*) $We = 1$, (*b*) $We = 2$, (*c*) $We = 5$, (*d*) $We = 10$, (*e*) region of stability for $n = 1$.

References

André, P. 2017 Interstellar filaments and star formation. *C. R. Geosci.* **349** (5), 187–197.

Benjamin, T.B. 1967 Shearing flow over a wavy boundary. *J. Fluid Mech.* **6** (2), 127–147.

Breysse, P.C., Kamionkowski, M. & Benson, A. 2014 Oscillations and stability of polytropic filaments. *Mon. Not. R. Astron. Soc.* **437** (1), 2675–2685.

CALDARELLI, M.M., DIAS, O.J.C., EMPARAN, R. & KLEMM, D. 2009 Black holes as lumps of fluid. *J. High Energy Phys.* **04**, 024.

CARDOSO, V. & DIAS, O.J.C. 2006 Rayleigh–Plateau and Gregor–Laflamme instabilities of black strings. *Phys. Rev. Lett.* **96**, 181601.

CHANDRASEKHAR, S. 1981 *The Gravitational Instability of an Infinite Cylinder*, pp. 516–523. Dover Books on Physics Series, vol. 1. Dover Publications.

CHANDRASEKHAR, S. & FERMI, E. 1953 Problems of gravitational stability in the presence of a magnetic field. *Astrophys. J.* **118**, 116–141.

CHANDRASEKHAR, S. & LEBOVITZ, N.R. 1964 Non-radial oscillations of gaseous masses. *Astrophys. J.* **140**, 1517–1528.

CHERNYAVSKY, A., KEVREKIDIS, P.G. & PELINOVSKY, D.E. 2018 Krein signature in Hamiltonian and $\mathbb{PT}$ -symmetric systems. *Springer Tracts Mod. Phys.* **280**, 465–491.

FREUNDLICH, J., JOG, C.J. & COMBES, F. 2014 Local stability of a gravitating filament: a dispersion relation. *Astron. Astrophys.* **564**, A7.

FUKUMOTO, Y. 2003 The three-dimensional instability of a strained vortex tube revisited. *J. Fluid Mech.* **493**, 287–318.

GILLIS, J. 1961 Stability of a column of rotating viscous liquid. In *Mathematical Proceedings of the Cambridge Philosophical Society*, vol. 57, pp. 152–159. AMS.

GILLIS, J. & KAUFMAN, B. 1962 The stability of a rotating viscous jet. *Q. Appl. Maths* **19** (4), 301–308.

HANSEN, C.J., AIZENMAN, M.L. & ROSS, R.L. 1976 The equilibrium and stability of uniformly rotating, isothermal gas cylinders. *Astrophys. J.* **207**, 736–744.

HENDERSON, K.L. & BARENGHI, C.F. 2002 The stability of a superfluid rotating jet. *J. Phys.* A*: Math. Gen.* **35** (45), 9645–9655.

HOCKING, L.M. 1960 The stability of a rigidly rotating column of liquid. *Mathematika* **7** (1), 1–9.

HOCKING, L.M. & MICHAEL, D.H. 1959 The stability of a column of rotating liquid. *Mathematika* **6** (1), 25–32.

KUBITSCHEK, J.P. & WEIDMAN, P.D. 2007*a* The effect of viscosity on the stability of a uniformly rotating liquid column in zero gravity. *J. Fluid Mech.* **572**, 261–286.

KUBITSCHEK, J.P. & WEIDMAN, P.D. 2007*b* Helical instability of a rotating viscous liquid jet. *Phys. Fluids* **19** (11), 114108.

KUBITSCHEK, J.P. & WEIDMAN, P.D. 2008 Helical instability of a rotating liquid jet. *Phys. Fluids* **20** (9), 091104.

MACKAY, R.S. & MEISS, J.D. 1987 *Stability of Equilibria of Hamiltonian Systems*, pp. 137–153. CRC Press.

MCKEE, C.F. & OSTRIKER, E.C. 2007 Theory of star formation. *Annu. Rev. Astron. Astrophys.* **45**, 565–687.

MILES, J.W. 1957 On the generation of surface waves by shear flows. *J. Fluid Mech.* **3** (2), 185–204.

MOORE, D.W. & SAFFMAN, P.G. 1975 The instability of a straight vortex filament in a strain field. *Proc. R. Soc. Lond.* A **346** (1646), 413–425.

MOTIEI, M.M., HOSSEINIRAD, M. & ABBASSI, S. 2021 Gravitational instability of non-isothermal filamentary molecular clouds in presence of external pressure. *Mon. Not. R. Astron. Soc.* **502** (4), 6188–6200.

NAGASAWA, M. 1987 Gravitational instability of the isothermal gas cylinder with an axial magnetic field. *Prog. Theor. Phys.* **77** (3), 635–652.

OSTRIKER, J. 1964*a* The equilibrium of polytropic and isothermal cylinders. *Astrophys. J.* **140**, 1056–1066.

OSTRIKER, J. 1964*b* On the oscillations and the stability of a homogeneous compressible cylinder. *Astrophys. J.* **140**, 1529–1546.

PEDLEY, T.J. 1967 The stability of rotating flows with a cylindrical free surface. *J. Fluid Mech.* **30** (1), 127–147.

PLATEAU, J.A.F. 1873 *Statique expérimentale et théorique des liquides soumis aux seules forces moléculaires*. Gauthier-Villars.

RAYLEIGH, LORD 1878 On the instability of jets. *Proc. Lond. Math. Soc.* **1** (1), 4–13.

ROSENTHAL, D.K. 1962 The shape and stability of a bubble at the axis of a rotating liquid. *J. Fluid Mech.* **12** (3), 358–366.

ROY, A., GARG, P., REDDY, J.S. & SUBRAMANIAN, G. 2021 Inertio-elastic instability of a vortex column. arXiv:2101.00805.

ROY, A. & SUBRAMANIAN, G. 2014 Linearized oscillations of a vortex column: the singular eigenfunctions. *J. Fluid Mech.* **741**, 404–460.

SADHUKHAN, S., MONDAL, S. & CHAKRABORTY, S. 2016 Stability of rotating self-gravitating filaments: effects of magnetic field. *Mon. Not. R. Astron. Soc.* **459** (3), 3059–3067.

STODÓLKIEWICZ, J.S. 1963 On the gravitational instability of some magneto-hydrodynamical systems of astrophysical interest. Part III. *Acta Astron.* **13**, 30–54.

TSAI, C.-Y. & WIDNALL, S.E. 1976 The stability of short waves on a straight vortex filament in a weak externally imposed strain field. *J. Fluid Mech.* **73** (4), 721–733.

WEIDMAN, P. 1994 Stability criteria for two immiscible fluids rigidly rotating in zero gravity. *Revue Roumaine Sci. Tech. Sér. Méc. Appl.* **39**, 481–496.

WEIDMAN, P.D., GOTO, M. & FRIDBERG, A. 1997 On the instability of inviscid, rigidly rotating immiscible fluids in zero gravity. *Z. Angew. Math. Phys.* **48** (6), 921–950.

ZEEMAN, E.C. 1976 Catastrophe theory. *Sci. Am.* **234** (4), 65–83.